ARTICLE IN PRESS

Available online at www.sciencedirect.com

SCIENCE DIRECT®

Thin Solid Films xx (2004) xxx–xxx

thin solid films

www.elsevier.com/locate/tsf

Structural study of a low dielectric thin film using X-ray reflectivity and grazing incidence small angle X-ray scattering

C.-H. Hsu[a,*], U-Ser Jeng[a], Hsin-Yi Lee[a], Chih-Mon Huang[a], K.S. Liang[a], D. Windover[b], T.-M. Lu[b], C. Jin[c]

[a]*National Synchrotron Radiation Research Center, Hsinchu, Taiwan, ROC*
[b]*Center for Integrated Electronics, Electronics Manufacturing and Electronic Media, Rensselaer Polytechnic Institute, Troy, NY, USA*
[c]*Texas Instruments, Dallas, TX, USA*

Received 30 December 2003; received in revised form 8 July 2004; accepted 16 July 2004

Abstract

We have studied the structure of a high-porous silica thin film with pore sizes in nanometer scale using X-ray reflectivity and small angle X-ray scattering in grazing incidence geometry. The reflectivity data provide the information of surface and interface characteristics, density–depth profile, and porosity of the xerogel film. Whereas the grazing incidence small angle X-ray scattering results reveal the internal structure of the porous film, including pore shape and size, and averaged inter-pore spacing. It is demonstrated that the combination of these two techniques is a powerful structural characterization tool to porous thin films.
© 2004 Published by Elsevier B.V.

Keywords: X-ray scattering; Structural properties; Dielectrics

1. Introduction

Low dielectric constant is one of the principal considerations in the selection of interlayer dielectric materials for advanced integrated circuit applications. The relatively high dielectric constant of SiO_2, around 4, will eventually preclude its use as an interlayer dielectric due to an increased R-C delay, high cross talk, as well as high noise and power dissipation. These disadvantages motivate the desire in developing new low-k materials that can be used as potential replacements for SiO_2. Currently, the Teflon family [1] and porous materials [2] are the two classes of materials having dielectric constants less than 2. In recent developments, porous materials have demonstrated many merits as a potential candidate for interlayer dielectric materials and attracted a great deal of attentions [3]. It is well known that the structures of porous materials influence strongly their electric properties and mechanical strength as well. For instance, a high porosity inevitably leads to a weak structure. In addition, as interlayer dielectrics, the pore sizes must be small as compared to the feature sizes of microelectronic devices, and uniformly distributed in the materials for practical applications. These requirements place strong demands on controlling and characterizing the microstructures of these porous thin films.

Various measurements, such as positron annihilation lifetime spectroscopy [4,5], ellipsometric porosimetry [6], small angle neutron scattering [7], off-specular X-ray reflectivity [8], have been conducted to investigate the average pore size and pore size distribution of porous low-k dielectric thin films. Even though small angle X-ray scattering (SAXS) has long been demonstrated to be advantageous in characterizing structures of nano-scale inhomogeneity in colloidal solutions and porous materials,

* Corresponding author. Tel.: +88 635 780 281x7118; fax: +88 635 783 813.
E-mail address: chsu@nsrrc.org.tw (C.-H. Hsu).

0040-6090/$ - see front matter © 2004 Published by Elsevier B.V.
doi:10.1016/j.tsf.2004.07.062

UNCORRECTED PROOF

it is rarely employed to study the structure of porous thin films. Conventionally, SAXS measurements are conducted in a transmission geometry. For porous materials in a form of thin films, it is difficult to obtain a decent SAXS intensity in such a geometry due to the short X-ray pass length in the materials. Moreover, the substrate absorption further diminishes the SAXS signals and may also introduce undesired background. All these factors hinder the application of SAXS in thin film studies. The difficulty can be overcome using SAXS in the grazing incidence geometry, as first demonstrated by Levine et al. [9,10]. In this study, we combine X-ray reflectivity [11] and grazing incidence small angle X-ray scattering (GISAXS) to investigate the microscopic structure of a sol–gel-derived silica xerogel film.

2. Experiment

A xerogel film was spun from an organic solvent containing slurry on a Si(001) wafer with a ~900 Å thick SiO_2 overlayer. The xerogel film was then cured through a sol–gel process and dried under atmospheric pressure. This ends with a xerogel film of approximate 5000 Å thick. The sample is subsequently undergone a proprietary surface treatment to prevent the film from moisture uptake. The xerogel composition was determined using Rutherford backscattering spectrometry to be $SiO_{2.2}C_{0.6}$. The Si and O ratios were determined using conventional modeling. The C ratio was determined using Carbon Nuclear Reaction Analysis to increase C signal-to-noise ratio. These ratios are known to be correct within approximately 5 at.% each. A sample of dimensions of 92×64 mm was used in this study.

X-ray scattering measurements were conducted at the wiggler beamline BL17B in the National Synchrotron Radiation Research Center. The beamline was equipped with a double-crystal monochromator, consisting of two Si(111) crystals to provide a monochromatic beam. Photons of 8 keV energy, corresponding to a wavelength λ of 1.55 Å, were used. Three pairs of slits were set up inside the experimental hutch to provide a collimated beam with dimensions of typical 0.6 mm×0.2 mm (H×V) at the sample position. The first two pairs of slits, 1 m apart, were used for major collimation whereas the third pair for minimizing parasite scattering. An eight-circle diffractometer was adapted, with which both in-plane and off-plane scans could be conveniently performed. Either a scintillation NaI counter or a position sensitive detector, which was located 815 and 960 mm from the sample position, respectively, was used.

A schematic of the scattering geometry is illustrated in Fig. 1, where the sample surface is defined as the x–y plane and the incident X-ray lies in the y–z plane. K_i, K_r and K_s denote incident, reflected, and scattered wave vectors, respectively, whereas α and β stand for incident and exit angles, respectively, and ϕ measures the scattering angle away from the y–z plane. The wave vector transfer $\boldsymbol{q}=(q_x, q_y, q_z)$ can be decomposed into three orthogonal components as follows: $q_x=(2\pi/\lambda)(\cos\beta\ \sin\phi)$, $q_y=(2\pi/\lambda)(\cos\beta\cos\phi-\cos\alpha)$ and $q_z=(2\pi/\lambda)(\sin\alpha+\sin\beta)$. For reflectivity measurements, the intensities of specularly reflected X-rays, i.e. $\alpha=\beta$ and $\phi=0$, are collected as a function of incident angle. The intensity variation vs. q_z, which equals to $4\pi\ \sin(\alpha)/\lambda$ in this case, provides the information about the laterally averaged electron density as a function of depth. Therefore, the density, thickness as well as the interfacial roughness of a thin film can be extracted from reflectivity results. On the other hand, GISAXS provides complementary information about the internal structure of the xerogel. In our measurements, the incident angle α is kept slightly larger than the critical angle of total external reflection, α_c, of the xerogel film, which is ~0.115°, and the scattered intensities are measured as a function of ϕ and β. In such a configuration, the incident angle is large enough to probe the interior of the film and meantime small enough to increase the X-ray path length within the film by orders of magnitude. For an incident angle ~0.2°, X-ray path length within a several thousand Angstroms thick film is several hundred microns. This significantly enhances the SAXS intensity from the thin film. The q dependence of the scattered intensity so obtained reveals the shape, size, and spatial correlation of the pore/wall structure within the porous film.

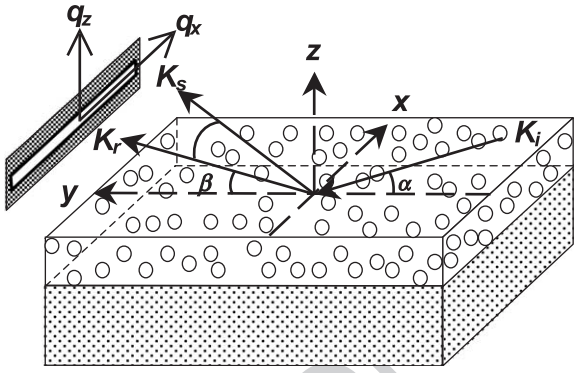

Fig. 1. A schematic of the GISAXS geometry.

3. Results and discussion

Fig. 2 displays a scanning electron microscopy (SEM) image of the xerogel film with a magnification of 50,000. It clearly exhibits the typical pore/wall two-phase topology, with a characteristic spacing of several hundreds Å roughly. However, it is difficult to identify the pore regions from the wall regions simply from the image taken. We then apply the scattering method to characterize the nano-structure of the xerogel film. Filled circles in Fig. 3 depict the high resolution X-ray reflectivity of the xerogel sample. The two maxima at q_z equal to 0.0157 and 0.030 $Å^{-1}$ are associated with the total external reflection occurred at air/xerogel and xerogel/SiO_2 interfaces, respectively. Due to the finite size

UNCORRECTED PROOF

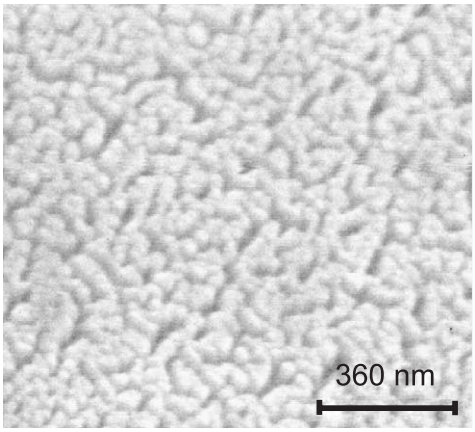

Fig. 2. SEM image of the surface morphology of the xerogel film.

of sample, part of the incident beam straddles over the sample surface at small incident angle, the footprint effect, resulting in the initial intensity rising at low q_z end of the reflectivity curve. Pronounced oscillations with a period Δq~0.001 Å^{-1} are observed for regions larger than the film critical angle. This is known as the Kiessig fringes originated from the interferences between X-rays reflected at different interfaces. The thickness of the film can be readily estimated from the oscillation period using $2\pi/\Delta q$. Also shown in the inset is the reflectivity curve collected up to q_z~0.25 Å^{-1}. A second set of oscillations with a larger period Δq~0.0066 Å^{-1} become the dominant feature for q_z>0.175 Å^{-1}, which corresponds to the Si oxide layer grown on Si substrate with a thickness of 908±7 Å.

To perform quantitative analysis, we adopt a model of n-layer structure on a Si substrate to simulate the reflectivity curve measured. Electron density, layer thickness and interfacial root-mean-square (rms) roughness of each layer are the fitting parameters. The Parratt recursion formalism [12] modified to incorporate the interface roughness is applied to calculate reflected intensity. The interface roughness is modeled by a density variation with an error function profile [13]. The calculated intensity is further convoluted with a Gaussian function to account for the instrument resolution. The obtained electron densities are converted to mass density with the known composition of each layer. The best fit of the high resolution reflectivity data with a two-layer model is plotted by the solid line in Fig. 3, which nicely reproduces the experimental data. Because reflectivity in low q_z range is more sensitive to the features with large length scale and the density profile close to the surface, there will be no discernable difference in the interested q_z range of the reflectivity if we further distinguish the underlying Si oxide layer from the Si substrate with similar density. Therefore, a two-layer model is sufficient to get a satisfactory fit for the structural information desired.

The best-fit two-layer model consists of a 5786±3 Å thick xerogel film and a 88±5 Å thick top layer. The average mass density of xerogel layer is ρ=0.61 g/cm^3 whereas the top layer has a slightly higher density, 0.84 g/cm^3, provided that its composition is the same as that of xerogel. The existence of the top layer is attributed to the surface treatment of xerogel to prevent it from moisture uptake. Similar observation has also been reported by Wu et al. [7]. Since the average density of the xerogel layer is the product of the skeletal density of silica ρ_s and the film porosity P, namely $\bar{\rho}=\rho_s(1-P)$, we thus determine the porosity of the xerogel film 63%, based on ρ_s=1.63 g/cm^3 reported by Lin et al. in a study of the similarly prepared xerogel films [14,15].

From the fitting results, we also learned that the roughness of sample surface is 52 Å, which reveals the large degree of raggedness of a porous surface. To further extract the information of the layers deep under, we tried to fit the reflectivity shown in the inset. However, due to the presence of many irregular fine features, especially in the middle q_z region, adding more layers to the best-fit two-layer model mentioned above is not sufficient to obtain a nice fit over the whole q_z range. Nevertheless, by fitting the slope of reflectivity curve, we determined the xerogel/Si oxide interface roughness to be approximate 15 Å, which is several times larger than what is expected for a Si oxide surface. This large number reflects not only the geometric roughness of the interface but also the density gradient from the SiO_2 to the porous xerogel film.

From the X-ray reflectivity data, we determined the density and thus the porosity of the xerogel film. To probe the size and shape of the pores, we further turned to the GISAXS measurements. Fig. 4 illustrates a two-dimensional contour map of the GISAXS intensity distribution above the reflected beam with α fixed at 0.25°. The data were collected using a linear detector lying in the x-direction and scanning along the z-direction. A disc-shaped beam stop mounted on a 1.5-mm-wide metal bar is used to mask

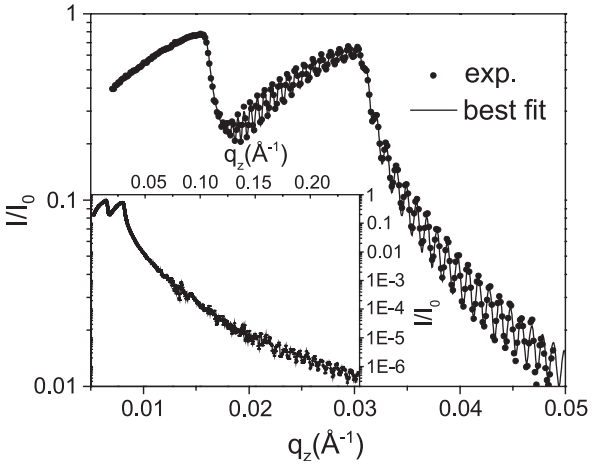

Fig. 3. Experimental data (●) and best fitted result (–) for the high resolution specular reflectivity of the xerogel/Si sample. The data are fitted using a two-layer model. The inset displays the reflectivity curve collected over a large q_z range. The oscillations at high q_z's correspond to a layer of about 910 Å thick.

UNCORRECTED PROOF

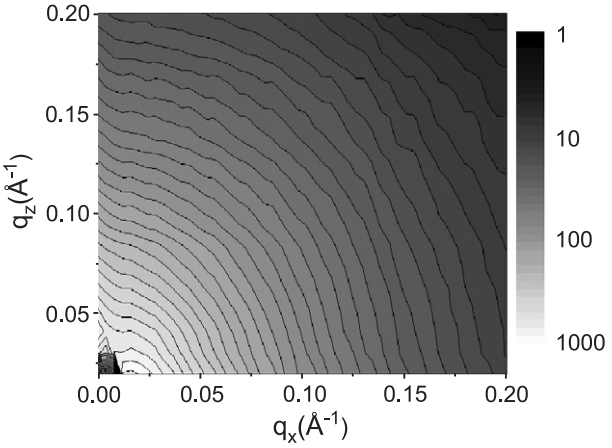

Fig. 4. Contour map of the GISAXS pattern for the xerogel film collected at α=0.25°.

the intense reflected beam and the straddled direct beam. The distortion of the scattering pattern in the region of q_x~0 is coming from the diffuse tail of reflected beam. Overall, the two-dimensional scattering pattern has a slightly deformed circular shape elongated along surface normal. This non-circular intensity distribution reveals that the internal structure of xerogel is not isotropic. This slight anisotropy is likely to be induced by the boundary condition imposed by the Si substrate during the formation of the xerogel film in sol–gel process.

Illustrated in Fig. 5 is the GISAXS intensity distribution as a function of q_x collected at α=0.2° and β=0.34°. Pronounced interference peak appears at q_x~0.0175 Å^{-1} which is a signature of the existence of a short range ordering between pores/walls. This interference peak was not noticed in our previous study [16] and only became clear with the improved resolution and lower reachable range in q_x, ~0.003 Å^{-1}. Be aware that β=0.34° is larger than both critical angles α_c(Si) and α_c(xerogel); this rules out the possibility that the peak comes from the surface diffuse scattering, the Yoneda wing [17]. Estimated from the peak position, the average inter-pore spacing is roughly 360 Å, which places an upper limit of the average inter-pore distance. This number is consistent with the characteristic length observed from the SEM image. Because α and β are always kept above the critical angle in our measurements, the region q_z<0.02 Å^{-1} is not accessible. This explains why the interference peak is not observed along the surface normal.

In sight of the presence of the interference peaks, we analyzed the GISAXS data with a model different from the random two-phase structure [14–16]. Even though it is difficult to describe the overall irregular morphology of porous materials using regular shapes, the local characteristics obtained in different length scales will still be helpful in establishing some sense of the shape and size of the pores/walls. Therefore, we fit the scattering intensity with models of different shapes, such as spheres, rods and disks. The Kratky–Prod plot of the GISAXS data collected at α=β=0.2° (open circles) is displayed in Fig. 6 and the curve follows a straight line in the region 0.0015 Å^{-2}<q_x^2<0.02 Å^{-2}. It is known that the scattering intensity of randomly orientated disk-like, or more properly flake-like in current case, particles in the middle-q region can be approximated by $I(q) \propto \exp(-q^2R_t^2)/q^2$, where R_t is the radius of gyration across the thickness of the disk and is equal to $T/\sqrt{12}$ for homogeneous disks [18,19]. As a comparison, we also show that the rod-like characteristic (solid line) from the same Kratky–Porod approximation in the inset, which does not fit the data as well. Deduced on the best-fit line shown in Fig. 6, the mean disk thickness is 28 Å. Moreover, the data deviate from straight line at q_x' ~0.039 Å^{-1} implying that the disk-like characteristics persists well up to ~160 Å ($2\pi/q_x'$) in the lateral direction of the disk. We have also analyzed the GISAXS intensity distribution along surface normal. From several GISAXS profiles collected at q_x=0.009–0.02 Å^{-1} and α_i=0.16–0.25°, we find the average disk thickness obtained from the Kratky–Porod plot is 27 Å and the lateral dimension of the disk is about 100 Å. This result indicates that disk size is slightly smaller along surface normal than parallel to the surface. We emphasize that this kind of anisotropy in structure is difficult to be probed by SAXS in transmission geometry.

In the high q region, the data show the characteristic of power-law scattering, $I(q_x) \sim q_x^{-a}$. The a=3.5 fitted indicates that these wall/pore interfaces have a fractal structure. This is a reasonable result for the porous materials made via sol–gel process.

Note, as the message conveyed from the Babinet principle, it is difficult to assign the small characteristic length measured to the pores or xerogel matrix. In principle, anomalous X-ray scattering can alter the atomic scattering factor of the same xerogel matrix and offer the similar effect as contrast variation. However, it is difficult to be apply anomalous X-ray scattering in this case because the low absorption-edge energy of the light consisting elements, e.g. 1.84 keV for Si K-edge. Another approach may help to resolve this problem is to conduct the GISAXS measure-

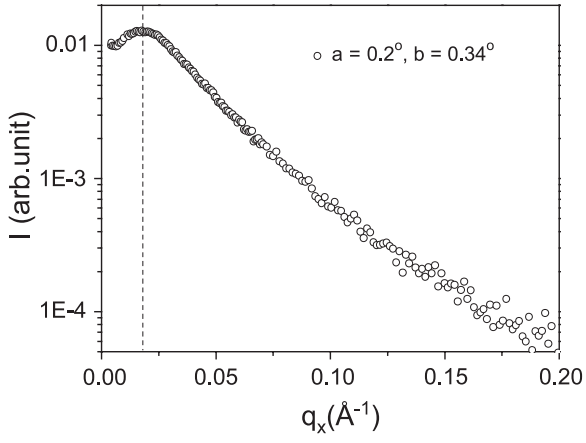

Fig. 5. GISAXS data of the xerogel/Si sample collected at α=0.2° and β=0.34°. The dashed line marks q_x=0.0175 Å^{-1}.

UNCORRECTED PROOF

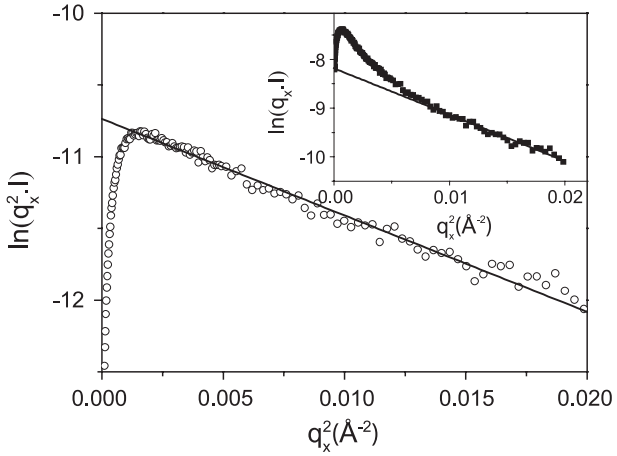

Fig. 6. The GISAXS data collected at α=0.2° and β=0.2° are fitted (solid line) using the Kratky–Porot approximation for the disk-like shape. In the inset, we show that the rod-like characteristic (dashed line) from the same Kratky–Porod approximation does not fit the data.

ment prior to and after the drying process of the xerogel film [3]. The solvent, which fills the pores, provides the necessary density variation as compared to the empty pores, to differentiate the pores from the matrix.

4. Conclusion

We have demonstrated that the combination of X-ray reflectivity and GISAXS is powerful in characterizing the structure of porous thin films. In this work, we applied these two X-ray techniques to study a low-*k* dielectric silica xerogel film grown on a Si wafer. From the results the density, porosity, pore shape, characteristic pore size and correlation length of the porous film are characterized under nondestructive condition. In addition, the GISAXS offers a readily mean to examine the degree of anisotropy of the film structure parallel and normal to the interface, which can hardly be obtained by other techniques.

Acknowledgements

This work is supported by the National Science Council of Republic of China under Contract No. NSC 91-2112-M-213-010.

References

[1] T.C. Nason, J.A. Moore, T.-M. Lu, Appl. Phys. Lett. 60 (1992) 1866, (and references therein).
[2] L.W. Hrubesh, L.E. Keene, V.R. Latorre, J. Mater. Res. 8 (1993) 1736, (and references therein).
[3] C. Jin, S. List, E. Zielinski, Mater. Res. Soc. Proc. 511 (1998) 213.
[4] D.W. Gidley, W.E. Frieze, T.L. Dull, A.F. Yee, C.V. Nguyen, H.M. Ho, Appl. Phys. Lett. 76 (2000) 1282.
[5] M.P. Petkow, M.H. Weber, K.G. Lynn, K.P. Rodbell, Appl. Phys. Lett. 77 (2000) 2470.
[6] M.R. Baklanov, K.P. Mofilnikov, V.G. Polovinkin, F.N. Dultsev, J. Vac. Sci. Technol., B 18 (2000) 1385.
[7] W.-L. Wu, W.E. Wallace, E.K. Lin, G.W. Lynn, C.J. Glinka, E.T. Ryan, H.-M. Ho, J. Appl. Phys. 87 (2000) 1193.
[8] K. Omote, Y. Ito, S. Kawamura, Appl. Phys. Lett. 82 (2003) 544.
[9] J.R. Levine, J.B. Cohen, Y.W. Chung, P. Geogopoulos, J. Appl. Crystallogr. 22 (1989) 528.
[10] J.R. Levine, J.B. Cohen, Y.W. Chung, Surf. Sci. 248 (1991) 215.
[11] D. Windover, T.-M. Lu, S.L. Lee, A. Kumar, H. Bakhru, C. Jin, W. Lee, Appl. Phys. Lett. 76 (2000) 158.
[12] L.G. Parratt, Phys. Rev. 95 (1954) 359.
[13] S.D. Kowowsky, C.-H. Hsu, P.S. Pershan, J. Bevk, B.S. Freer, Appl. Surf. Sci. 84 (1995) 179.
[14] E.K. Lin, W.-L. Wu, C. Jin, J.T. Wetzel, Mater. Res. Soc. Symp. Proc. 612 (2000) D4.1.
[15] W.-L. Wu, E.K. Lin, C. Jin, J.T. Wetzel, Mater. Res. Soc. Symp. Proc. 612 (2000) D5.22.
[16] C.-H. Hsu, H.-Y. Lee, K.S. Liang, U.-S. Jeng, D. Windover, T.-M. Lu, C. Jin, Mater. Res. Soc. Symp. Proc. 612 (2000) D5.23.
[17] S.K. Sinha, E.B. Sirota, S. Garoff, H.B. Stanley, Phys. Rev., B 38 (1988) 2297.
[18] O. Glatter, O. Kratky, Small Angle X-ray Scattering, Academic Press, New York, NY, 1982.
[19] T.-L. Lin, Physica, B 180 (1992) 505.

UNCORRECTED PROOF